JOURNAL OF SOLID STATE CHEMISTRY 73, 603–609 (1988)

Complex Copper(II) Fluorides

IX. Weberite-Related $NaCu_3F_7$: The First Fluoride with Copper Both in Square Planar and Octahedral Coordination*

JEAN RENAUDIN, MARC LEBLANC, AND GÉRARD FEREY

Laboratoire des Fluorures, UA CNRS 449, Faculté des Sciences, Route de Laval, 72017 Le Mans Cedex, France

AND ARIEL DE KOZAK AND MAURICE SAMOUËL

Laboratoire de Cristallochimie du Solide, Université P. et M. Curie, Tour 54, 4 Place Jussieu, 75252 Paris Cedex 05, France

Communicated by E. F. Bertaut, February 25, 1988

$NaCu_3F_7$ is monoclinic (space group $C2/c$): a = 12.124(6) Å, b = 7.344(4) Å, c = 6.924(4) Å, β = 120.59(4)°, Z = 4. The structure is refined from 751 independent reflections to R = 0.047 (R_w = 0.050). Copper ions occupy one square planar and two octahedral sites; sodium ions adopt a distorted cubic coordination. The three-dimensional network is closely related to the orthorhombic weberite structural type and corresponds to a frustrating triangular topology of the magnetic sublattice on which exist both ferro- and antiferromagnetic superexchange interactions. © 1988 Academic Press, Inc.

Introduction

The chemical and X-ray crystallographic studies of the ternary system $NaF–BaF_2–CuF_2$ (*2*) have evidenced two new phases: $NaCu_3F_7$ and $Na_4BaCu_3F_{12}$. In the binary diagram $NaF–CuF_2$, only $NaCuF_3$ (*3*) and Na_2CuF_4 (*4*) were previously studied. This paper describes the crystal structure of the heptafluoride which is compared to the orthorhombic weberite structural type. The superexchange magnetic interactions on the frustrating topology of Cu^{2+} cations are analyzed.

* For parts I to VIII, see Refs. (*1*, *2*).

Experimental

Single crystals were obtained under the conditions described elsewhere (*2*). A very thin blue-green platelet (with the largest face indexed {100}) was selected for X-ray data collection on an AED2 Siemens-STOE automated four-circle diffractometer. The experimental conditions and crystallographic characteristics are summarized in Table I. The great number of rejected reflections (67%) is explained by the very small dimensions of the crystal and by the large angular range of measurement (θ_{max} = 45°). The collected intensities were corrected for Lorentz-polarization effects as well as for absorption (Gaussian integra-

0022-4596/88 $3.00

TABLE I

CRYSTALLOGRAPHIC CHARACTERISTICS AND EXPERIMENTAL CONDITIONS FOR X-RAY DATA COLLECTION

Symmetry: Monoclinic (space group: $C2/c$)
Cell parameters[a] (from 16 reflections within range $27 < 2\theta < 35°$):
a = 12.124(7) Å, b = 7.344(5) Å, c = 6.924(5) Å, β = 120.59(4)°
V = 530.7 Å^3, Z = 4, M = 346.60 g · mole^{-1}
Density: 4.33 g · cm^3 (calculated); 4.35 g · cm^3 (experimental)
Crystal size: 0.055 × 0.050 × 0.010 mm^3
Radiation: Mo$K\alpha$ (λ = 0.71073 Å)
Linear absorption coefficient: 121.2 cm^{-1}
Transmission factors: A_{max} = 0.879; A_{min} = 0.740
Standard reflections: −804/−444/800 measured every 60 min
Intensity standard deviation: 2.5% max
Range: $2 < \theta < 45°$, $-26 \le h \le 26$, $0 \le k \le 15$, $-14 \le l \le 14$
40 steps per reflection, 4 sec per step, step width: 0.03°
Measured reflections = 5803
Rejected reflections = 3914 (with $I/\sigma(I) < 5$)
Independent reflections = 751 (R_{int} = 0.043)
Number of refined parameters: 58
Weighting scheme: $w = 3.6/(\sigma(F)^2 + 5 \times 10^{-4} F^2)$
Secondary extinction: 5(2) × 10^{-8}
Fourier difference map:
maximum height = 2.8 e$^-$ Å^{-3}
minimum height = −2.0 e$^-$ Å^{-3}

[a] These cell parameters differ from the previous study (*2*); the transformation matrix is:

$$\begin{bmatrix} 1 & 0 & 2 \\ 0 & -1 & 0 \\ 0 & 0 & -1 \end{bmatrix}.$$

tion). Atomic scattering factors and anomalous dispersion corrections were taken from the "International Tables for X-Ray Crystallography" (*5*) for Na^+, Cu^{2+}, and F^- ions.

Structure Resolution

The structure was solved from the options TREF and PATT of the SHELXS-86 program (*6*) and all refinement calculations were performed using the SHELX-76 program (*7*) on a D.E.C. MicroVAX-II computer. Two copper sites were first located on 4a and 4c positions of space group $C2/c$: this led to a reliability factor R = 0.35. A Fourier map then revealed the positions of the third copper (site 4d) and sodium (site 4b): R = 0.19. The F^- ions were located from successive Fourier syntheses. The refinement of atomic parameters and isotropic temperature factors smoothly converged to R = 0.077 (R_w = 0.079). The residual fell to R = 0.047 (R_w = 0.050) when applying anisotropic thermal motion. It is noteworthy that the maximum residual peaks in the final Fourier difference map are in the vicinity of Cu(3) ions. Table II presents the final results for the eight independent positions. The list of structure factors may be obtained on request to one of the authors (G.F.).

Description of the Structure

Until now, the main difference between the crystal chemistry of copper oxides (*8*) and fluorides was the coexistence of several types of coordination for copper in the former (see, for instance, high T_c superconductors) and only one type (octahedra or, more rarely, square planes) for the latter. $NaCu_3F_7$ is the first example of coexistence of two different coordination polyhedra for cupric ions in fluorine chemistry: the fluorine octahedra around Cu(1) and Cu(2) are classically elongated by the Jahn–Teller effect whereas—this is the most striking feature of the structure—Cu(3) ions adopt a square planar coordination of F(2) and F(3) ions (Table III). The structural formula of the basic building unit Cu_3F_7 is therefore $[Cu(1)F(1)_{2/2}F(2)_{2/3}F(4)_{2/2}]$ $[Cu(2)F(1)_{2/2}F(2)_{2/3}F(3)_{2/2}]$ $[Cu(3)F(2)_{2/3}F(3)_{2/2}]$. However, the next-nearest neighbors F(1) and F(4) of Cu(3) can also be taken into account despite the long distances: nearly 2.9 Å

TABLE II

STRUCTURAL AND THERMAL PARAMETERS ($\times 10^4$) WITH ESTIMATED STANDARD DEVIATIONS IN PARENTHESES[a]

Atom	Site	x/a	y/b	z/c	U_{11}	U_{22}	U_{33}	U_{12}	U_{13}	U_{23}	B_{eq} (Å^2)
Na	4b	0	½	0	249(23)	285(24)	268(23)	7(34)	190(20)	9(37)	1.90(30)
Cu(1)	4a	0	0	0	112(4)	99(4)	91(4)	−3(9)	65(3)	−14(9)	0.75(5)
Cu(2)	4c	¼	¼	0	79(6)	112(10)	80(7)	−8(6)	44(6)	−23(6)	0.70(9)
Cu(3)	4d	¼	¼	½	190(9)	102(11)	179(9)	14(7)	138(8)	23(7)	1.08(12)
F(1)	8f	0976(6)	2025(9)	0044(12)	173(20)	160(22)	330(28)	−44(22)	195(22)	−40(19)	1.50(31)
F(2)	8f	3292(5)	2992(9)	3186(11)	150(20)	251(24)	110(18)	−33(18)	83(16)	−57(20)	1.28(25)
F(3)	8f	1579(6)	4664(7)	4014(11)	234(22)	75(20)	219(21)	18(14)	147(19)	29(15)	1.28(28)
F(4)	4e	0	1070(13)	¼	656(61)	193(37)	200(33)	0	323(40)	0	2.38(57)

[a] $B_{eq} = \frac{4}{3} \Sigma_i \Sigma_j B_{ij} (a_i \cdot a_j)$ (*17*).

TABLE III

SELECTION OF INTERATOMIC DISTANCES (Å) AND BOND ANGLES

Na polyhedron				
Na–F(3)	2 × 2.353(7)			
Na–F(3)	2 × 2.453(4)			
Na–F(1)	2 × 2.476(5)			
Na–F(2)	2 × 2.837(5)	⟨Na–F⟩ = 2.530		
Cu(1) octahedron				Angle at Cu(1)
Cu(1)–F(1)	2 × 1.891(6)	2 × F(1)–F(4)	2.617(4)	87.4(4)°
Cu(1)–F(4)	2 × 1.898(3)	2 × F(4)–F(2)	2.712(6)	79.4(4)°
Cu(1)–F(2)	2 × 2.319(5)	2 × F(1)–F(4)	2.740(8)	92.6(4)°
		2 × F(1)–F(2)	2.824(7)	83.6(5)°
⟨Cu(1)–F⟩	= 2.036	2 × F(2)–F(1)	3.152(7)	96.4(4)°
Cu(2) octahedron				Angle at Cu(2)
Cu(2)–F(1)	2 × 1.897(6)	2 × F(1)–F(2)	2.634(6)	86.4(5)°
Cu(2)–F(2)	2 × 1.949(6)	2 × F(3)–F(1)	2.736(6)	80.9(4)°
Cu(2)–F(3)	2 × 2.296(7)	2 × F(1)–F(2)	2.803(5)	93.6(4)°
		2 × F(2)–F(3)	2.930(7)	86.9(4)°
		2 × F(3)–F(2)	3.091(5)	93.1(3)°
⟨Cu(2)–F⟩	= 2.047	2 × F(1)–F(3)	3.201(8)	99.1(4)°
Cu(3) polyhedron				Angle at Cu(3)
Cu(3)–F(3)	2 × 1.862(4)	2 × F(2)–F(3)	2.697(7)	89.8(4)°
Cu(3)–F(2)	2 × 1.956(4)	2 × F(2)–F(3)	2.705(6)	90.2(3)°
⟨Cu(3)–F⟩	= 1.909			
Cu(3)–F(4)	2 × 2.822(4)			
Cu(3)–F(1)	2 × 2.979(7)			

Cu–Cu distances		Superexchange angles	
Cu(1)–Cu(1)	3.462	Cu(1)–F(4)–Cu(1)	131.6°
Cu(2)–Cu(3)	3.462	Cu(2)–F(2)–Cu(3)	124.8°
Cu(1)–Cu(3)	3.544	Cu(1)–F(2)–Cu(3)	111.7°
Cu(1)–Cu(2)	3.544	Cu(1)–F(1)–Cu(2)	138.7°
Cu(2)–Cu(3)	3.672	Cu(2)–F(3)–Cu(3)	123.7°
Cu(1)–Cu(2)	3.724	Cu(1)–F(2)–Cu(2)	121.2°

TABLE IV

VALENCE BOND ANALYSIS OF $NaCu_3F_7$ USING THE ZACHARIASEN LAW[a]

	F(1)	F(2)	F(3)	F(4)	Σ	$\Sigma_{theo.}$
Cu(1)	2 × 0.454	2 × 0.143	—	2 × 0.445	2.08	2
Cu(2)	2 × 0.446	2 × 0.388	2 × 0.152	—	1.97	2
Cu(3)	2 × 0.024	2 × 0.380	2 × 0.490	2 × 0.037	1.86	2
Na	2 × 0.119	2 × 0.056	2 × 0.153 2 × 0.125	—	0.91	1
Σ	1.04	0.97	0.92	0.96		

[a] $s = \frac{1}{3}e^{(2.005-d_i)/0.37}$ for Cu–F and $s = \frac{1}{6}e^{(2.313-d_i)/0.48}$ for Na–F (*9*).

compared to 2.3 Å for the elongation axes of the octahedra. Indeed the valence bond analysis (*9*) shows that these Cu–F distances account for 6% in the balance (Table IV). Therefore the square plane becomes to some extent a distorted cube (Fig. 1). This is important for the structural correlations described in the last section. In the crystal chemistry of copper fluorides, only $CaCuF_4$, $SrCuF_4$, and Sr_2CuF_6 (*10, 11*) exhibit such an environment.

From [010] projection (Fig. 2), the structure can be considered as a succession of layers parallel to the (*h*00) planes which correspond to the main faces of the platelet. The first type of layer (at $x = \frac{1}{4}$ or $\frac{3}{4}$) is built up from Cu(2) octahedra and Cu(3) square planes which form together a distorted bidimensional network like a defect perovskite (Fig. 3a). The second layer (at $x = 0$ or $\frac{1}{2}$) is composed of two kinds of infinite chains running along the *c*-axis: a *trans* chain of corner-sharing Cu(1) octahedra (in which elongation axes of two consecutive octahedra are orthogonal) linked to a chain of edge-sharing Na cubes (Fig. 3b). These different layers are connected by vertices in such a way that the three copper polyhedra form a triangular cationic sublattice (Fig. 4). Therefore the corresponding topology is frustrating and this point will be developed in the next section from the magnetic point of view.

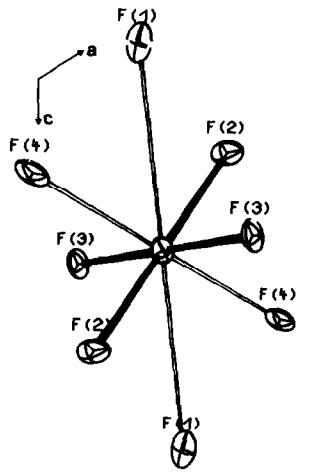

FIG. 1. ORTEP drawing (*18*) of the Cu(3) environment: the short bonds are filled.

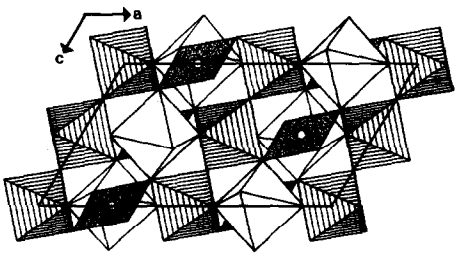

FIG. 2. The (010) projection of $NaCu_3F_7$ using the program STRUPLO (*19*). Cu(1) octahedra are hatched and Cu(3) square planes are dot-shaded.

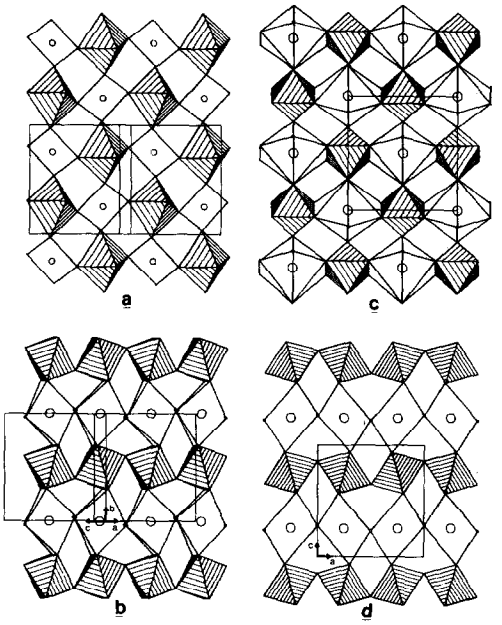

FIG. 3. Comparison between the two kinds of layers in $NaCu_3F_7$ (a, b) and in the orthorhombic weberites $Na_2M^{2+}M^{3+}F_7$ (c, d). Sodium ions are represented by large circles.

Discussion

With this new result, an unexpected structural trend appears within the binary system NaF–CuF_2. In contrast to the BaF_2–CuF_2 diagram in which the ratio of edge-sharing octahedra increases with the Cu content when Cu/Ba > 1/1 (*12*), no edge-sharing occurs in $NaCu_3F_7$ which is the closest compound to rutile CuF_2 in the system NaF–CuF_2; on the contrary, it is found for the copper-poor region with Na_2CuF_4 structure, which is described by isolated rutile chains (*4*).

Beside their close chemical formulas, the structures of $NaCu_3F_7$ and of the orthorhombic weberites $Na_2M^{2+}M^{3+}F_7$ (*13, 14*) (space group *Imma*) are very similar. Indeed, $NaCu_3F_7$ may be described in the pseudo-orthorhombic cell ($a_0 = c$, $b_0 = a + c$, $c_0 = b$, and $\gamma = 83°$) with space group $I112/a$ which is a subgroup of $I2/m2/m2/a$. If we remember that sodium ions adopt two types of eightfold coordination in the weberite (i.e., a cube and a hexagonal bipyramid), the structural relations are obvious when considering the two kinds of layers described above: the packing of *trans* chains $[NaCu(1)F_4]^{-1}$ and $[NaM^{2+}F_4]^{-1}$, with Na inside cubes, is strictly identical in $NaCu_3F_7$ (Fig. 3b) and $Na_2M^{2+}M^{3+}F_7$ (Fig. 3d). The other kind of layer, formulated $[Cu(2)Cu(3)F_3]^{+1}$ in $NaCu_3F_7$ (Fig. 3a), becomes $[NaM^{3+}F_3]^{+1}$ in the weberite because the hexagonal bipyramid of sodium in $[Na_2M^{2+}M^{3+}F_7$ (Fig. 3c) replaces the distorted cube of Cu(3) after some rotation of the single octahedra. Therefore the correlative formulation of $NaCu_3F_7$ can be written [Na–Cu(3)][Cu(1)–Cu(2)]F_7 from the comparison with $[Na_2][M^{2+}M^{3+}]F_7$.

Two important features arise from the (001) projection of the structure (Fig. 4). Infinite *trans* chains of Cu(1) and Cu(2) octahedra appear along the [−110] direction at the $z = 0$ level and along [110] at $z = \frac{1}{2}$. In these chains, the elongation axes of the octahedra are roughly parallel and arranged in a ferrodistortive way. This would lead to an antiferromagnetic coupling in these chains, the superexchange pathway involving ex-

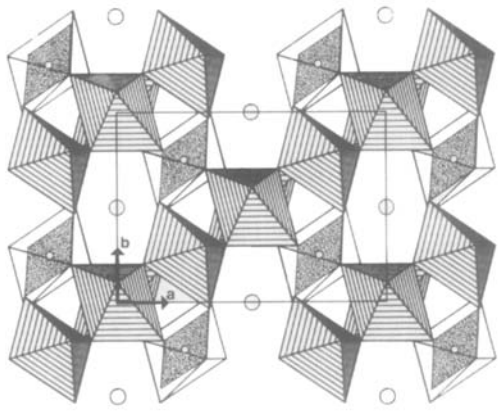

FIG. 4. Projection of $NaCu_3F_7$ along the *c*-axis showing the ferrodistortive arrangement of elongated octahedra. Sodium ions are represented by large circles.

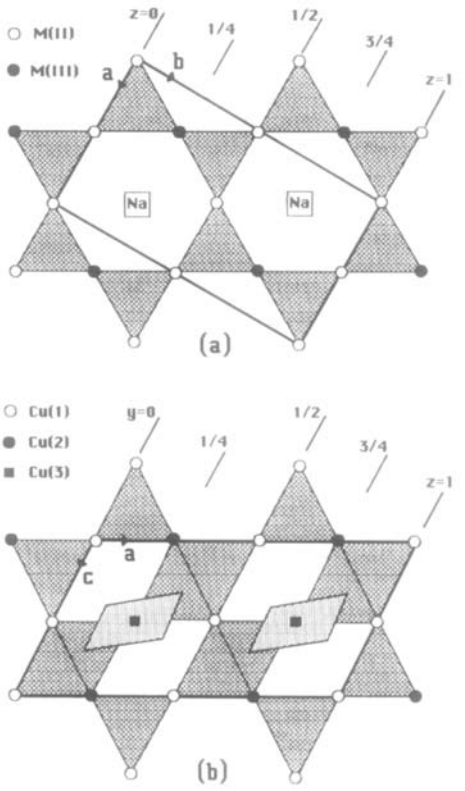

FIG. 5. Comparison of the magnetic subnetworks in the (0−11) plane for the weberite (a) and (−110) for $NaCu_3F_7$ (b).

clusively the $d_{x^2-y^2}$ orbitals (*15*) and the d_{z^2} orbitals pointing toward the F^- ions of the square plane around Cu(3). Therefore ferromagnetic interactions are expected via d_{z^2}–p–$d_{x^2-y^2}$ between Cu(1) or Cu(2) and Cu(3). The second feature, already evoked at the end of the description, comes from the connection between two parallel *trans* chains via Cu(3) square planes: the complete copper subnetwork draws triangular cycles. Consequently, $NaCu_3F_7$ must exhibit an enhanced frustrating magnetic topology when compared to that of the weberite. In the latter, triangular platelets surround hexagonal ones in the (110) and (−110) planes (Fig. 5a) and build up a "kagome plane net" (noted 3.6.3.6 using the Schläfli symbol (*16*)) of magnetic cations. In the former, Cu(3) occupies the center of the above hexagons and induces two additional triangular platelets, i.e., a (3.4.3.4, $3^2.4.3^2.4$) plane net (Fig. 5b). The existence of a frustrating topology on which ferro- and antiferromagnetic interactions are involved must lead to a very interesting magnetic behavior study which is currently in progress both on $NaCu_3F_7$ and substituted compounds.

Acknowledgment

The authors are very indebted to Dr. J. Pannetier for his help in valence bond analysis and his critical reading of the manuscript.

References

1. J. RENAUDIN, G. FEREY, A. DE KOZAK, AND M. SAMOUËL, *Rev. Chim. Miner.* **24,** 295 (1987), and references therein.
2. A. DE KOZAK, M. SAMOUËL, J. RENAUDIN, AND G. FEREY, submitted for publication.
3. W. RÜDORFF, G. LINCKE, AND D. BABEL, *Z. Anorg. Allg. Chem.* **320,** 150 (1963).
4. D. BABEL, *Z. Anorg. Allg. Chem.* **336,** 200 (1965).
5. J. A. IBERS AND W. C. HAMILTON, Eds., "International Tables for X-Ray Crystallography," Vol. IV, Kynoch Press, Birmingham (1974).
6. G. M. SHELDRICK, SHELXS-86, *in* "Crystallographic Computing 3" (G. M. Sheldrick, C. Krüger, and R. Goddard, Eds.), pp. 175–189, Oxford Univ. Press, London/New York (1985).
7. G. M. SHELDRICK, "SHELX-76: A Program for Crystal Structure Determination," Cambridge (1976).
8. B. RAVEAU, *Proc. Indian Natl. Sci. Acad. A* **52,** 67 (1986).
9. G. FEREY, M. LEBLANC, A. DE KOZAK, M. SAMOUËL, AND J. PANNETIER, *J. Solid State Chem.* **56,** 288 (1985), and references therein.
10. H. G. VON SCHNERING, B. KOLLOCH, AND A. KOLODZIEJCZYK, *Angew. Chem.* **12,** 440 (1971).
11. R. VON DER MÜHLL, D. DUMORA, J. RAVEZ, AND P. HAGENMULLER, *J. Solid State Chem.* **2,** 262 (1970).
12. J. RENAUDIN, G. FEREY, A. DE KOZAK, AND M. SAMOUËL, *Rev. Chim. Miner.* **23,** 497 (1986).
13. Y. LALIGANT, G. FEREY, G. HEGER, AND J. PANNETIER, *Z. Anorg. Allg. Chem.* **553,** 163 (1987), and references therein.

14. S. KUMMER, Thesis, Marburg (1986).
15. D. REINEN AND C. FRIEBEL, *Structure Bonding* **37,** 1 (1979).
16. M. O'KEEFFE AND B. G. HYDE, *Philos. Trans. R. Soc. London, Ser. A* **295,** 553 (1980), and references therein.
17. W. C. HAMILTON, *Acta Crystallogr.* **12,** 609 (1959).
18. C. K. JOHNSON, "ORTEP-II," Oak Ridge National Laboratory (1971).
19. R. X. FISCHER, STRUPLO-84, *J. Appl. Crystallogr.* **18,** 258 (1985).